Reaction between Graphene Oxide and Intracellular Glutathione Affects Cell Viability and Proliferation

Baojin Ma, Shi Guo, Yuta Nishina, Alberto Bianco

Reaction between Graphene Oxide and Intracellular Glutathione Affects Cell Viability and Proliferation

Journal:	*ACS Applied Materials & Interfaces*
Manuscript ID	am-2020-17523u.R2
Manuscript Type:	Article
Date Submitted by the Author:	n/a
Complete List of Authors:	Ma, Baojin; CNRS, UPR3572, Immunophatologie et Chimie Thérapeutiques Guo, Shi; CNRS, UPR3572, Immunophatologie et Chimie Thérapeutiques Nishina, Yuta; Okayama University , Research Core for Interdisciplinary Sciences Bianco, Alberto; CNRS, UPR3572, Immunophatologie et Chimie Thérapeutiques

Reaction between Graphene Oxide and Intracellular Glutathione Affects Cell Viability and Proliferation

*Baojin Ma, Shi Guo, Yuta Nishina, Alberto Bianco**

B. Ma, S. Guo, A. Bianco

CNRS, Immunology, Immunopathology and Therapeutic Chemistry, UPR3572, University of Strasbourg, ISIS, Strasbourg, 67000, France

E-mail: a.bianco@ibmc-cnrs.unistra.fr

Y. Nishina

Graduate School of Natural Science and Technology, Okayama University, Tsushimanaka, Kita-ku, Okayama, 700-8530, Japan

Research Core for Interdisciplinary Sciences, Okayama University, Tsushimanaka, Kita-ku, Okayama, 700-8530, Japan

Keywords: carbon nanomaterial, reduction, oxidation, reactive oxygen species, cancer cells

ABSTRACT: Graphene oxide (GO) is currently developed for biomedical applications as a promising nanoplatform for drug delivery, phototherapy and biosensing. As a consequence, its safety and cytotoxicity issues have attracted enormous attention. It has been demonstrated that GO causes an increase of intracellular oxidative stress, likely leading to its cytotoxicity and inhibition of cell proliferation. Being one of the main reductive intracellular substances, glutathione (GSH) is vital in the regulation of the oxidative stress level to maintain normal cellular functions. In this study, we found that GSH could be oxidized to GSSG by GO, leading to the formation of reduced GO (rGO). GSH depletion affects the intracellular reductive/oxidative balance, provoking the increase of ROS level, sequentially inhibiting cell viability and proliferation. Therefore, the reaction between GO and GSH provides a new perspective to explain the origin of GO cytotoxicity.

INTRODUCTION

Graphene oxide (GO) was broadly used like a platform in the biomedical domain for drug delivery, photothermal therapy, biosensing, or tissue engineering thanks to its excellent physicochemical properties, biocompatibility and biodegradability.[1-3] For example, GO functionalized with a chemotactic peptide was able to deliver doxorubicin efficiently for cancer therapy, and could be biodegraded by myeloperoxidase through the induced neutrophil degranulation.[4] Luminol-functionalized and silver nanoparticle-decorated GO was used to detect aflatoxin M1 as a sensitive electrochemiluminescence biosensor.[5] In view of these applications, it is mandatory to assess the toxicity and biosecurity of GO.[6,7]

Many reports have demonstrated that GO possesses low cytotoxicity even at high concentrations. Especially purified GO was found to display low cytotoxic effects (up to a concentration of 100 μg/mL) *in vitro*, and does not provoke inflammatory effects or formation of granuloma *in vivo*.[8,9] Currently, the general belief is that the increase of the level of reactive oxygen species (ROS) produced by GO is the main reason for its cytotoxicity.[10-12] GO-caused ROS could damage the mitochondria and activate apoptosis/autophagy.[13] It has been reported that the oxidation degree of GO surface, surface charge and the amount of carbon radicals have significant influence in determining the damages of cell membrane, the peroxidation of lipids, and the cellular toxicity.[14-16] Notably, a double mechanism, implying an uncontrolled production of hydroxyl radicals and the generation of intermediates involved in the oxidation of cytochrome c, was put forward to explain the toxicity of GO induced by stress in *C. elegans*.[17] However, until now, a detailed study about a direct reaction between GO and

intracellular reductive molecules (especially glutathione, GSH) to explain the cytotoxicity of this material was missing.

It is recognized that GSH has a fundamental role in regulating intracellular oxidation/reduction balance. Few studies reported that molecules with thiol groups could reduce GO,[18-20] meaning that GO could oxidize intracellular GSH. Very recently, Wang *et al.* described the impact of GO epoxides on the mechanism of direct oxidation of the thiol groups in GSH at the atomic scale using density functional theory.[21] However, this study did not establish a direct connection between GO-mediated GSH oxidation and cell viability.

In our study, we found that GO could be reduced by GSH at physiological temperature, consequently oxidizing GSH to GSSG. Meanwhile, a little amount of GSH was covalently linked to rGO to form rGO-GSH. This allowed us to establish the association between GO-mediated intracellular GSH oxidation and cell impact. After incubation with GO at different concentrations, the viability and proliferation of HeLa cells slightly diminished. Meanwhile, the value of the intracellular GSH/GSSG ratio decreased and the content of ROS increased. The GSH depletion affected the oxidation-reduction balance, leading to an increase of ROS level, sequentially reducing the viability and inhibiting proliferation (**Figure 1**). Therefore, the reaction between GO and GSH suggests a new paradigm on the origin of GO cytotoxicity.

Figure 1. Illustration of the scheme of the reaction between GO and intracellular GSH.

RESULTS AND DISCUSSION

Reaction between GO and GSH. To imitate the intracellular reaction between GO and GSH, GO was incubated with GSH at physiological temperature (37°C). Raman measurement was performed to characterize the reduction degree of GO. Meanwhile, FT-IR spectra and thermogravimetric (TG) curves were acquired to show the surface functional group changes. Following the addition of GSH, the color of GO gradually changed from typical brown to black, providing a visual proof of the redox reaction between GO and GSH (**Figure 2**a, inset). The shift of absorbance spectra of rGO-GSH to higher wavelength (from ~230 nm to ~260 nm) also proved the reduction of GO (Figure 2a).[22,23] The increase of I_D/I_G value in Raman spectra suggests the formation of new small graphene domains after the reduction of GO (Figure 2b), similar to previous reports.[24,25] These results evidence the reduction of GO into rGO by GSH. Furthermore, the influence of pH and temperature on the reaction between GO and GSH was evaluated. Changes of the color and absorbance of the conjugate were observed and measured (Figure S1). It is clear that a high temperature accelerates the reaction rate, while pH has a slight effect on the reaction.

The starting GO and its reduced form were also characterized by FT-IR (Figure 2c). The peak at ~1727 cm^{-1} was assigned to C=O stretching band of carboxylic or carbonyl groups.[26] The peaks at ~1227 cm^{-1} and ~1048 cm^{-1} correspond to epoxy and alkoxy groups, respectively.[27] The peak at ~1623 cm^{-1} was attributed to carbon-carbon vibrations of non-oxidized graphitic domains.[28] After reduction with GSH, the intensity of the bands of the oxygenated functional groups obviously decreased, meaning that some of these groups on GO surface have been reduced by GSH. Besides, we did not observe -SH band at ~2515 cm^{-1},[29,30] confirming that almost no free GSH molecules were adsorbed onto GO surface (Figure S2). Furthermore, TG analysis allowed to show that the main weight loss of GO and rGO-GSH took place at ~220 ℃ and ~200 ℃, respectively. This is related to the removal of the labile functional groups (Figure 2d).[20] Besides, there was a second main weight loss of rGO-GSH at ~260 ℃ (Figure 2d, blue arrow), which could be attributed to covalently connected GSH on the surface of rGO (*vide infra*).[31] According to transmission electron microscopy (TEM) results, GO resulted well dispersed (Figure 2e), and the average size is ~500 nm measured by ImageJ (Figure S3). In contrast, rGO-GSH appeared more aggregated (Figure 2f). Therefore, we can conclude again that GO was reduced to rGO-GSH after reacting with GSH.

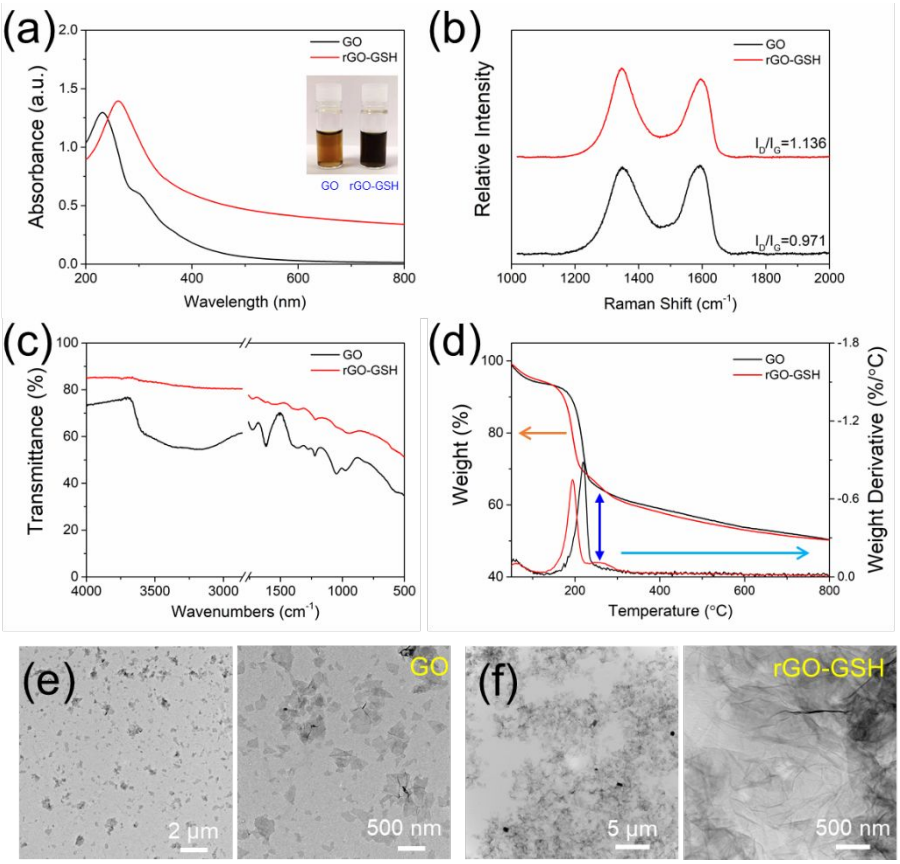

Figure 2. Characterization of the redox reaction between GO and GSH at 37 °C for 6 h. (a) Absorbance spectra (inset shows the digital picture of GO and rGO-GSH). (b) Raman spectra. (c) FI-IR spectra. (d) TG-DTA curves. (e) TEM images of GO at different magnification. (f) TEM images of rGO-GSH at different magnification.

Characterization of surface properties. Next, we analyzed the nature of the functional groups on the surface of GO and rGO-GSH by X-ray photoelectron spectroscopy (XPS). Compared to GO, the O/C ratio of rGO-GSH decreased from 46.9% to 38.1% (Figure S4). In the high-resolution spectrum, the area of the C-C/C=C band increased from 37.9% (GO) to 42.6% (rGO-GSH). Inversely, the area of the C-O and C=O peaks decreased from 45.8% to 40.2% and from 13.8% to 7.2%, respectively, after GO reacted with GSH (**Figure 3**a and c). Therefore, some of oxygenated functional groups were eliminated by reduction with GSH.[32,33] In addition, we

have also evidenced the presence of S-O bonds introduced onto GO surface during the sulfuric acid treatment used for the preparation of GO from graphite (Figure 3b). Notably, a new small peak was observed at ~163.5 eV, and attributed to S−C bond. The appearance of this peak confirmed the opening of the ring epoxides by the thiol group of GSH (Figure 3d).[20,34,35] Therefore, combined with the results of FT-IR analysis, we can conclude that a little amount of GSH was covalently bound to the surface of rGO.

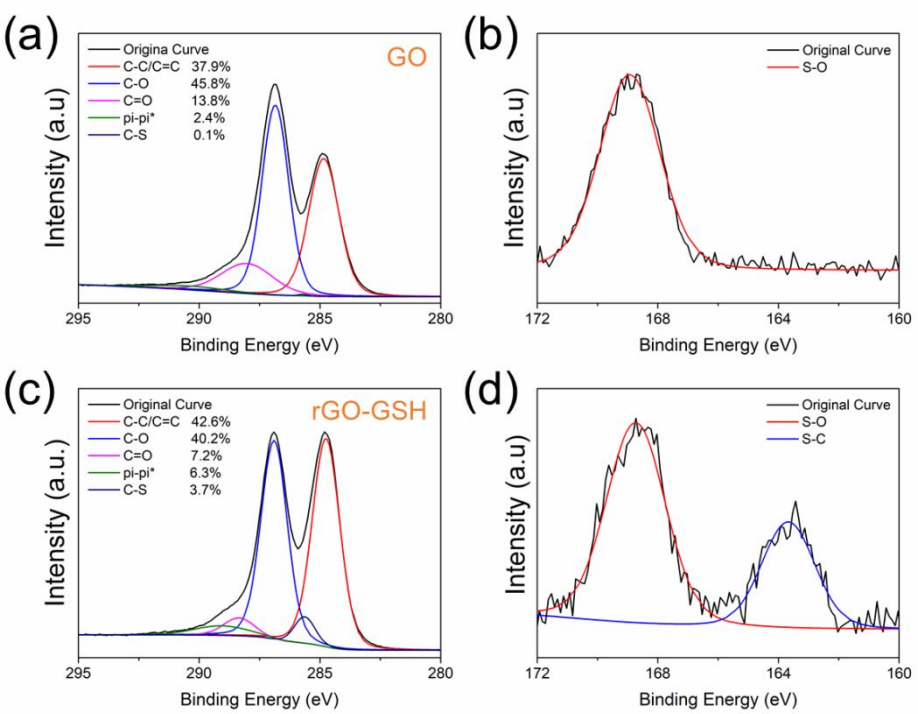

Figure 3. High resolution XPS spectra of GO and rGO-GSH. (a) and (b) high-resolution C1s and S2p of GO. (c) and (d) high-resolution C1s and S2p of rGO-GSH.

GSH oxidation triggered by GO. To further confirm the type of products generated during the reaction between GO and GSH, HPLC spectra of the supernatant were measured. Comparing the HPLC spectra of starting GSH and GSH maintained at 37 °C for 6 h, the peak at ~3.4 min corresponds indeed to the same molecule (Figure S5a and b). This means that GSH

is not oxidized in the absence of GO under the same reaction conditions. However, a strong new peak at ~5.2 min appeared in the HPLC spectrum of the supernatant after GSH reacted with GO, corresponding to GSSG (Figure S5c).[36] Meanwhile, the peak intensity of GSH decreased consistently. Therefore, GSH was oxidized into GSSG by GO. In order to confirm which functional groups (e.g. SH or NH_2) are responsible for the reduction of GO, the single amino acids constituting GSH sequence were reacted with GO. GSH contains glycine, glutamic acid, and cysteine. GO was mixed with glutamic acid (having one amino and two carboxylic groups) and cysteine (having one amino, one carboxylic, and one thiol group) at 37 °C for 6 h. There was almost no color change of GO dispersion after mixed with glutamate (Figure S6). However, cysteine could reduce GO into rGO, and the color of the GO dispersion turned from brown to black, which is consistent with a previous study.[18] Meanwhile, the area of the C-C/C=C increased to 43.1%, and the area of the C-O and C=O decreased to 49.2% and 5.8%, respectively, after GO reacted with cysteine according to the high resolution XPS spectra of C1s (Figure S7a). Furthermore, there was also a new peak appeared at ~163.5 eV (S−C bond) (Figure S7b), which is consistent with the results of rGO-GSH. Therefore, the SH group, rather than NH_2 or COOH, is involved in the reaction with GO during the redox process.

Effect of GO on cell viability and proliferation. We then decided to study the effect of GO on viability and proliferation of cancer cells. For this purpose, HeLa cells were cultured with GO at different concentration for 24 h and 48 h. The viability of HeLa cells was quantified by MTS test. As shown in **Figure 4**a and b, GO displayed low cytotoxicity to HeLa cells. Even at highest concentrations of 100 μg/mL, HeLa cell viability was still higher than 80% after 48 h.

According to the bright field images (Figure S8a and b), although GO could inhibit cell proliferation to a certain extent, cells still kept a good state and displayed a normal morphology. In addition, there were only a few dead cells both in the control group and GO treated group according to live/dead staining results (Figure 4c). The relative fluorescence intensity of live cells stained by calcein AM also confirmed that GO displays low cytotoxicity to HeLa cells (Figure S9), consistent with MTS results. This low cytotoxicity could be attributed to the intracellular self-regulation,[37,38] ensuring the biosafety of GO. Therefore, GO can only slightly inhibit HeLa cell viability and proliferation. Many reports have demonstrated that GO is able to inhibit the viability and proliferation of different types of cancer cells, comprising HeLa, MCF-7, HepG2, SW480, and others, although the inhibition levels were found different.[39-41] Consequently, the reaction between intracellular GSH and GO can happen in different cancer cell lines. In this context, we decided to measure the influence of GO on the viability of MCF-7 cells. It is clear that GO reduces MCF-7 cell viability, similarly to HeLa cells (Figure S10).

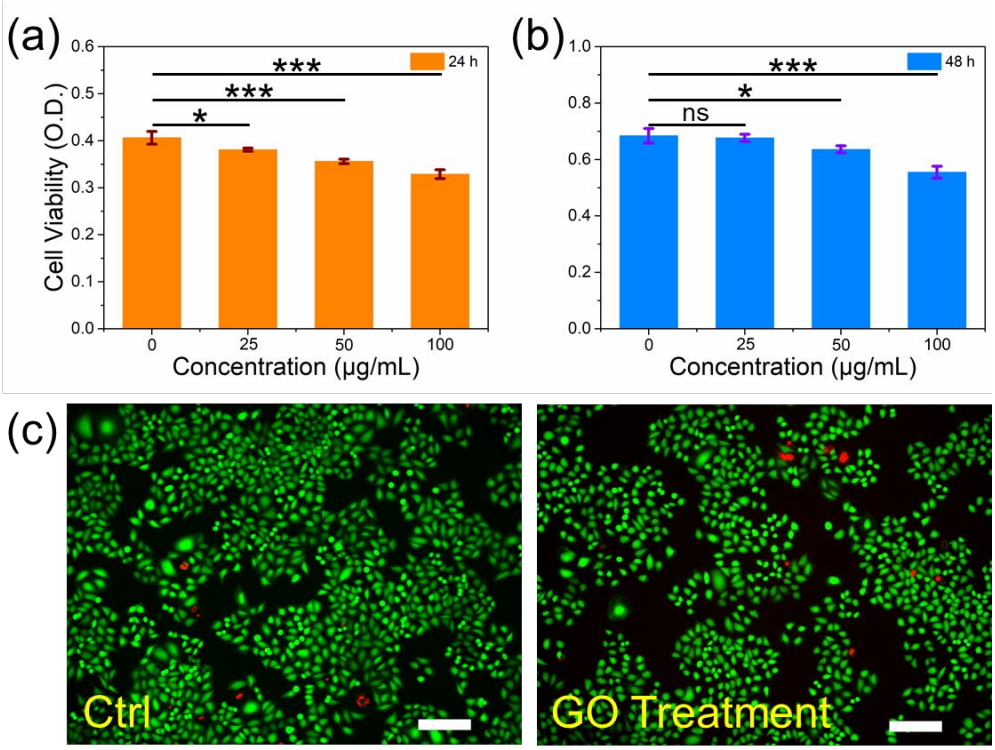

Figure 4. Cytotoxicity of GO under different concentration. (a) and (b) GO incubated with HeLa cells for 24 and 48 h, respectively. (c) Live/dead staining of HeLa cells after GO treatment for 24 h (GO concentration=100 μg/mL). The scale bar is 200 μm (*$p < 0.05$; **$p < 0.01$; ***$p < 0.001$).

To evaluate the impact of GO on normal cell lines, human keratinocyte HaCaT cells were chosen and treated with GO. Due to the low level of GSH and reduced uptake, GO shows relatively lower toxicity to these cells. After 48 h, we evidenced that GO slightly affected the viability of HaCaT cells at the highest concentration tested (corresponding to 100 μg/mL) (Figure S11). So, GO can also regulate the viability of normal cells by reacting with intracellular GSH, although the effects are weaker than that on cancer cells.

GO causes GSH depletion and ROS increase. In the next experiment, the ratio between GSH and GSSG inside HeLa cells before and after GO treatment was measured to confirm the intracellular reaction between GO and GSH. As shown in **Figure 5**a, the intracellular GSH/GSSG ratio decreased after GO treatment. This means that GO reacted with endogenous GSH after GO penetration into HeLa cells, leading to a decrease of the ratio between GSH and GSSG. Meanwhile, we measured the content of intracellular ROS to further show the change of ROS-associated oxidative stress, caused by GO. The ROS level significantly increased after GO treatment (Figure 5b). These data evidence that GO provoke an intracellular depletion of GSH and an increase of ROS, leading to a certain degree of cytotoxicity. GSH is the main reductive substance that regulates the balance of the intracellular reductive/oxidative

processes.[42,43] When GSH is depleted, ROS generated during physiological functions cannot be neutralized. As a consequence, an accumulation of ROS occurs. Several previous studies have confirmed that the accumulated ROS can provoke the impairment of DNA, proteins, and lipids, leading to deleterious effects on cell viability, proliferation, and death.[44-47]

In addition, the increased degree of ROS content was higher than the decrease of GSH, meaning that the reaction between GO and intracellular GSH is just one of the reasons for the increase of GO-triggered oxidative stress. Furthermore, the concentration of intracellular GSH is up to ~10 mM,[48] which is comparable with the reaction concentration of GSH in the test tube (~13 mM). Therefore, it can be hypothesized that intracellular GSH reacts with GO in the same way that happened in the test tube. Previous studies showed that GO inhibited implanted B16 tumor in a mouse model,[49] and could inhibit CT26 tumor growth, enhance cell death, autophagy, and immune cell infiltration.[50] Thus, it is reasonable to think that the proposed hypothesis most likely works in tumor models.

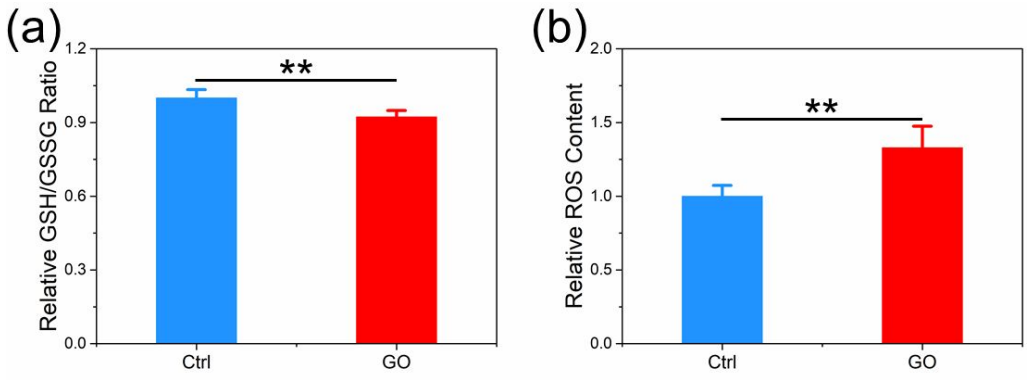

Figure 5. Change of intracellular ratio between GSH and GSSG (a) and ROS content (b) before and after GO (50 μg/mL) treatment for 24 h (*$p < 0.05$; **$p < 0.01$).

CONCLUSIONS

In summary, GSH could be oxidized to GSSG by GO, along with the formation of rGO-GSH at 37 ℃. Correspondingly, *in vitro* results uncovered that the intracellular GSH/GSSG ratio decreased and ROS content increased after GO treatment. As the main reductive substance, the depletion of GSH would further lead to an increase of ROS caused by GO, subsequently reducing cell viability and proliferation. Therefore, the redox reaction between GO and GSH shows a new viewpoint on the origin of the cytotoxicity of GO. We also believe that GO could act as adjuvant in enhancing cancer therapy by depleting intracellular GSH, although not proved yet.

EXPERIMENTAL MATERIALS AND METHODS

Materials. GO was prepared using the modified Hummers method and purified by dialysis at least for 10 days. GSH, glutamate and cysteine were purchased from Sigma-Aldrich. All chemicals were of analytical grade and used without purification.

Reaction between GO and GSH. Five mL of GO dispersion (1 mg/mL) and 20 mg of GSH were mixed at 37 °C for 6 h. The concentration of GSH is about 13 mM. Then, the obtained rGO-GSH was washed by deionized water for at least 6 times by centrifugation. The reactions between GO and glutamic acid and cysteine were performed under the same conditions. To measure absorbance spectra of rGO-GSH, rGO-GSH was sonicated for 60 min to get a homogeneous dispersion.

Characterization. The absorbance spectra were obtained using a Varian Cary winUV 50 Bio-spectrophotometer. Raman spectra were measured by a Renishaw inVia microscope

equipped with 532 nm laser. FT-IR spectra were obtained on a Perkin Elmer Spectrum One ATR-FT-IR spectrometer. TGA analysis was performed by TGA1 (Mettler Toledo) apparatus from 30 to 800 °C with a ramp of 10 °C/min under N_2 atmosphere using a flow rate of 50 mL/min and platinum pans. Morphological analysis was obtained by transmission electron microscope (TEM, Hitachi 7500, Hitachi High Technologies Corporation, Tokyo, Japan). XPS spectra were measured by a Thermo Scientific K-Alpha X-ray photoelectron spectrometer with a basic chamber pressure of 10^{-8} to 10^{-9} bar with an anode using Al Kα radiation (hv= 1486.6 eV).

Cell Viability. HeLa (human cervical adenocarcinoma) cells were cultured in high-glucose Dulbecco's modified Eagle medium (H-DMEM) with 10 μg/mL gentamycin (Lonza BioWhittaker), 10 mM N-(2-hydroxyethyl)-piperazine-N′-ethanesulfonic acid (Lonza BioWhittaker), 0.05 mM β-mercaptoethanol (Lonza BioWhittaker) and 10% fetal bovine serum (FBS). MCF-7 (human breast cancer) cells were cultured in RPMI 1640 medium with 10 μg/mL gentamycin (Lonza BioWhittaker), 10 mM N-(2-hydroxyethyl)-piperazine-N′-ethanesulfonic acid (Lonza BioWhittaker), 0.05 mM β-mercaptoethanol (Lonza BioWhittaker) and 10% FBS. HaCaT (human keratinocyte) cells were cultured in H-DMEM with the addition of 10% FBS, 10^{-2} M L-glutamine, 10^{-4} g/mL penicillin and 10^{-4} g/mL streptomycin. All cells were maintained under a humidified atmosphere of 5% CO_2 at 37 °C, and the culture medium was changed every 2 days. Cell viability was measured by MTS Assay Kit following manufacturer's instructions. Live/dead staining were performed by live/dead staining Kit following manufacturer's instructions. Bright field images were obtained by an inverted microscope.

Intracellular GSH/GSSG Ratio and ROS Content. The measurement of intracellular GSH/GSSG ratio and ROS content was performed by GSH/GSSG-Glo™ assay Kit (Promega Corporation) and reactive oxygen species (ROS) molecular probes™ CM-H2DCFDA (Thermal Fisher Scientific) according to the corresponding manufacturer's instructions. For GSH/GSSG ratio measurement, old medium in 96-well plate containing GO with different concentration was removed, and cells were washed by PBS. Fifty μL per well of Total GSH Lysis Reagent or GSSG Lysis Reagent was added. Then, the plate was shaken at room temperature for 5 min. The cell lysis solution was centrifuged at 4 °C for 20 min, and the supernatant was transferred into opaque 96-well plate. Fifty μL per well of Luciferin Generation Reagent was added to all wells. After shaking plate briefly, the plate was incubated at room temperature for 30 min. Finally, 100 μL per well of Luciferin Detection Reagent was added and the luminescence was measured after 15 min. For ROS content measurement, HeLa cells was stained with 10 μM CM-H2DCFDA work solution for 30-60 min at 37 °C. After washing by PBS, the fluorescence was measured by Varioskan™ LUX multimode microplate reader at Ex485 nm/Em525 nm.

Statistical Analysis. The statistical significance of the differences was determined by one-way ANOVA. Values with $P < 0.05$ were considered statistically significant ($*p < 0.05$, $**P < 0.01$, and $***P < 0.001$).

ASSOCIATED CONTENT

Supporting Information

The Supporting Information is available free of charge at https://pubs.acs.org/doi/

Absorbance spectra of GO after reacted with GSH at different pH and temperature (Figure S1), magnification region of FT-IR spectra (Figure S2), size distribution of GO (Figure S3), XPS survey full spectra (Figure S4), HPLC analysis (Figure S5), color change of GO after reaction with cysteine (Figure S6), high resolution XPS spectra of rGO after reacted with cysteine (Figure S7), bright field images of HeLa cells after GO treatment (Figure S8), the relative fluorescence intensity of live cells (Figure S9), viability of MCF-7 cells after GO treatment (Figure S10), viability and bright filed images of HaCaT cells after GO treatment (Figure S11). (PDF)

AUTHOR INFORMATION

Corresponding Author

Alberto Bianco – *CNRS, Immunology, Immunopathology and Therapeutic Chemistry, UPR3572, University of Strasbourg, ISIS, Strasbourg, 67000, France; E-mail: a.bianco@ibmc-cnrs.unistra.fr*

Authors

Baojin Ma – *CNRS, Immunology, Immunopathology and Therapeutic Chemistry, UPR3572, University of Strasbourg, ISIS, Strasbourg, 67000, France*

Shi Guo – *CNRS, Immunology, Immunopathology and Therapeutic Chemistry, UPR3572, University of Strasbourg, ISIS, Strasbourg, 67000, France*

Yuta Nishina – Graduate School of Natural Science and Technology, Okayama University, Tsushimanaka, Kita-ku, Okayama, 700-8530, Japan; Research Core for Interdisciplinary

Sciences, Okayama University, Tsushimanaka, Kita-ku, Okayama, 700-8530, Japan

Notes

The authors declare no competing financial interest.

ACKNOWLEDGMENTS

We gratefully acknowledge the Centre National de la Recherche Scientifique (CNRS) through the International Research Project MULTIDIM between I2CT Unit and Okayama University, the International Center for Frontier Research in Chemistry (icFRC), and financial support from the Agence Nationale de la Recherche (ANR) through the LabEx project Chemistry of Complex Systems (ANR-10-LABX-0026_CSC). We wish to thank Cathy Royer and Valérie Demais for help with TEM analyses at the "Plateforme Imagerie in vitro" at the Center of Neurochemistry (INCI, Strasbourg, France).

REFERENCES

(1) Yang, K.; Feng, L.; Shi, X.; Liu, Z. Nano-graphene in Biomedicine: Theranostic Applications. *Chem. Soc. Rev.* **2013,** *42*, 530−547.

(2) Reina, G.; González-Domínguez, J. M.; Criado, A.; Vázquez, E.; Bianco, A.; Prato, M. Promises, Facts and Challenges for Graphene in Biomedical Applications. *Chem. Soc. Rev.* **2017,** *46*, 4400−4416.

(3) Ma, B.; Martín, C.; Kurapati, R.; Bianco A. Degradation-by-design: How Chemical Functionalization Enhances the Biodegradability and Safety of 2D Materials. *Chem. Soc. Rev.*

2020, *49*, 6224−6247.

(4) Martín, C.; Ruiz, A.; Keshavan, S.; Reina, G.; Murera, D.; Nishina, Y.; Fadeel, B.; Bianco, A. A Biodegradable Multifunctional Graphene Oxide Platform for Targeted Cancer Therapy. *Adv. Funct. Mater.* **2019,** *29*, 1901761.

(5) Khoshfetrat, S. M.; Bagheri, H.; Mehrgardi, M. A. Visual Electrochemiluminescence Biosensing of Aflatoxin M1 Based on Luminol-functionalized, Silver Nanoparticle-decorated Graphene Oxide. *Biosens. Bioelectron.* **2018,** *100*, 382−388.

(6) Bianco, A. Graphene: Safe or Toxic? The Two Faces of the Medal. *Angew. Chem. Int. Ed.* **2013,** *52*, 4986−4997.

(7) Akhavan, O.; Ghaderi, E. Toxicity of Graphene and Graphene Oxide Nanowalls against Bacteria. *ACS Nano* **2010,** *4*, 5731−5736.

(8) Zhang, H.; Peng, C.; Yang, J.; Lv, M.; Liu, R.; He, D.; Fan, C.; Huang, Q. Uniform Ultrasmall Graphene Oxide Nanosheets with Low Cytotoxicity and High Cellular Uptake. *ACS Appl. Mater. Interfaces* **2013,** *5*, 1761−1767.

(9) Ali-Boucetta, H.; Bitounis, D.; Raveendran-Nair, R.; Servant, A.; Van den Bossche, J.; Kostarelos, K. Purified Graphene Oxide Dispersions Lack in vitro Cytotoxicity and in vivo Pathogenicity. *Adv. Healthc. Mater.* **2013,** *2*, 433−441.

(10) Hu, X.; Ouyang, S.; Mu, L.; An, J.; Zhou, Q. Effects of Graphene Oxide and Oxidized Carbon Nanotubes on the Cellular Division, Microstructure, Uptake, Oxidative Stress, and Metabolic Profiles. *Environ. Sci. Technol.* **2015,** *49*, 10825−10833.

(11) Zhang, W.; Yan, L.; Li, M.; Zhao, R.; Yang, X.; Ji, T.; Gu, Z.; Yin, J.-J.; Gao, X.; Nie, G. Deciphering the Underlying Mechanisms of Oxidation-state Dependent Cytotoxicity of

Graphene Oxide on Mammalian Cells. *Toxicol. Lett.* **2015,** *237*, 61−71.

(12) Li, Y.; Liu, Y.; Fu, Y.; Wei, T.; Le Guyader, L.; Gao, G.; Liu, R.-S.; Chang, Y.-Z.; Chen, C. The Triggering of Apoptosis in Macrophages by Pristine Graphene through the MAPK and TGF-beta Signaling Pathways. *Biomaterials* **2012,** *33*, 402−411.

(13) Tang, Z.; Zhao, L.; Yang, Z.; Liu, Z.; Gu, J.; Bai, B.; Liu, J.; Xu, J.; Yang, H. Mechanisms of Oxidative Stress, Apoptosis, and Autophagy Involved in Graphene Oxide Nanomaterial Anti-osteosarcoma Effect. *Inter. J. Nanomed.* **2018,** *13*, 2907.

(14) Li, R.; Guiney, L. M.; Chang, C. H.; Mansukhani, N. D.; Ji, Z.; Wang, X.; Liao, Y.-P.; Jiang, W.; Sun, B.; Hersam, M. C. Surface Oxidation of Graphene Oxide Determines Membrane Damage, Lipid Peroxidation, and Cytotoxicity in Macrophages in a Pulmonary Toxicity Model. *ACS Nano* **2018,** *12*, 1390−1402.

(15) Pieper, H.; Chercheja, S.; Eigler, S.; Halbig, C. E.; Filipovic, M. R.; Mokhir, A. Endoperoxides Revealed as Origin of the Toxicity of Graphene Oxide. *Angew. Chem. Int. Ed.* **2016,** *55*, 405−407.

(16) Wang, A.; Pu, K.; Dong, B.; Liu, Y.; Zhang, L.; Zhang, Z.; Duan, W.; Zhu, Y. Role of Surface Charge and Oxidative Stress in Cytotoxicity and Genotoxicity of Graphene Oxide towards Human Lung Fibroblast Cells. *J. Appl. Toxicol.* **2013,** *33*, 1156−1164.

(17) Zhang, W.; Wang, C.; Li, Z.; Lu, Z.; Li, Y.; Yin, J. J.; Zhou, Y. T.; Gao, X.; Fang, Y.; Nie, G. Unraveling Stress-induced Toxicity Properties of Graphene Oxide and the Underlying Mechanism. *Adv. Mater.* **2012,** *24*, 5391−5397.

(18) Wang, Y.; Xiao, Y.; Gao, G.; Chen, J.; Hou, R.; Wang, Q.; Liu, L.; Fu, J. Conductive Graphene Oxide Hydrogels Reduced and Bridged by L-cysteine to Support Cell Adhesion and

Growth. *J. Mater. Chem. B* **2017,** *5*, 511−516.

(19) Pham, T. A.; Kim, J. S.; Kim, J. S.; Jeong, Y. T. One-step Reduction of Graphene Oxide with L-glutathione. *Colloids Surf. A Physicochem. Eng. Asp.* **2011,** *384*, 543−548.

(20) Guo, S.; Nishina, Y.; Bianco, A.; Ménard-Moyon, C. A Flexible Method for Covalent Double Functionalization of Graphene Oxide. *Angew. Chem. Int. Ed.* **2020,** *59*, 1542-1547.

(21) Wang, Y.; Basdogan, Y.; Zhang, T.; Lankone, R. S.; Wallace, A.; Fairbrother, D. H.; Keith, J. A.; Gilbertson, L. M. Unveiling the Synergistic Role of Oxygen Functional Groups in the Graphene-Mediated Oxidation of Glutathione. *ACS Appl. Mater. Interfaces* **2020**. DOI: 10.1021/acsami.0c11539.

(22) Gurunathan, S.; Han, J. W.; Park, J. H.; Eppakayala, V.; Kim, J.-H. Ginkgo Biloba: a Natural Reducing Agent for the Synthesis of Cytocompatible Graphene. *Inter. J. Nanomed.* **2014,** *9*, 363.

(23) Gurunathan, S.; Han, J. W.; Dayem, A. A.; Eppakayala, V.; Kim, J.-H. Oxidative Stress-Mediated Antibacterial Activity of Graphene Oxide and Reduced Graphene Oxide in Pseudomonas Aeruginosa. *Inter. J. Nanomed.* **2012,** *7*, 5901.

(24) Wang, H.; Robinson, J. T.; Li, X.; Dai, H. Solvothermal Reduction of Chemically Exfoliated Graphene Sheets. *J. Am. Chem. Soc.* **2009,** *131*, 9910−9911.

(25) Moon, I. K.; Lee, J.; Ruoff, R. S.; Lee, H. Reduced Graphene Oxide by Chemical Graphitization. *Nat. Commun.* **2010,** *1*, 1−6.

(26) Liu, C.; Qiu, S.; Du, P.; Zhao, H.; Wang, L. An Ionic Liquid–Graphene Oxide Hybrid Nanomaterial: Synthesis and Anticorrosive Applications. *Nanoscale* **2018,** *10*, 8115−8124.

(27) Satheesh, K.; Jayavel, R. Synthesis and Electrochemical Properties of Reduced Graphene

Oxide via Chemical Reduction Using Thiourea as a Reducing Agent. *Mater. Lett.* **2013,** *113*, 5−8.

(28) Wang, S.; Wang, X. Microwave-assisted One-pot Synthesis of Metal/Metal Oxide Nanoparticles on Graphene and Their Electrochemical Applications. *Electrochim. Acta* **2011,** *56* (9), 3338−3344.

(29) Naji-Tabasi, S.; Razavi, S. M. A.; Mehditabar, H. Fabrication of Basil Seed Gum Nanoparticles as a Novel Oral Delivery System of Glutathione. *Carbohydr. Polym.* **2017,** *157*, 1703−1713.

(30) Huang, H.; Li, H.; Feng, J.-J.; Feng, H.; Wang, A.-J.; Qian, Z. One-pot Green Synthesis of Highly Fluorescent Glutathione-stabilized Copper Nanoclusters for Fe^{3+} Sensing. *Sens. Actuators B Chem.* **2017,** *241*, 292−297.

(31) Farrag, M., Preparation, Characterization and Photocatalytic Activity of Size Selected Platinum Nanoclusters. *J. Photochem. Photobiol. A* **2016,** *318*, 42−50.

(32) Zhou, Y.; Bao, Q.; Tang, L. A. L.; Zhong, Y.; Loh, K. P. Hydrothermal Dehydration for the “green” Reduction of Exfoliated Graphene Oxide to Graphene and Demonstration of Tunable Optical Limiting Properties. *Chem. Mater.* **2009,** *21*, 2950−2956.

(33) Yu, M.; Zhang, S.; Chen, Y.; Jin, H.; Zhang, Y.; Lu, L.; Shu, Z.; Hou, S.; Xie, B.; Cui, H. A Green Method to Reduce Graphene Oxide with Carbonyl Groups Residual for Enhanced Electrochemical Performance. *Carbon* **2018,** *133*, 101−108.

(34) Mellon, M.; Mangadlao, J.; Advincula, R.; Pentzer, E. The pH Dependent Reactions of Graphene Oxide with Small Molecule Thiols. *RSC Adv.* **2018,** *8*, 18388−18395.

(35) Luong, N. D.; Johansson, L. S.; Campell, J.; Seppälä, J. Functional Graphene by Thiol-ene

Click Chemistry. *Chem. Eur. J.* **2015,** *21* (8), 3183−3186.

(36) Zitka, O.; Skalickova, S.; Gumulec, J.; Masarik, M.; Adam, V.; Hubalek, J.; Trnkova, L.; Kruseova, J.; Eckschlager, T.; Kizek, R. Redox status expressed as GSH: GSSG ratio as a marker for oxidative stress in paediatric tumour patients. *Oncol. Lett.* **2012,** *4*, 1247−1253.

(37) Valko, M.; Leibfritz, D.; Moncol, J.; Cronin, M. T.; Mazur, M.; Telser, J. Free Radicals and Antioxidants in Normal Physiological Functions and Human Disease. *Int. J. Biochem. Cell B.* **2007,** *39*, 44−84.

(38) Nie, H.; Jing, J.; Tian, Y.; Yang, W.; Zhang, R.; Zhang, X. Reversible and Dynamic Fluorescence Imaging of Cellular Redox Self-Regulation using Fast-responsive Near-infrared Ge-Pyronines. *ACS Appl. Mater. Interfaces* **2016,** *8,* 8991−8997.

(39) Kutwin, M.; Sawosz, E.; Jaworski, S.; Wierzbicki, M.; Strojny, B.; Grodzik, M.; Ewa Sosnowska, M.; Trzaskowski, M.; Chwalibog, A. Nanocomplexes of Graphene Oxide and Platinum Nanoparticles against Colorectal Cancer Colo205, HT-29, HTC-116, SW480, Liver Cancer HepG2, Human Breast Cancer MCF-7, and Adenocarcinoma LNCaP and Human Cervical Hela B Cell Lines. *Materials* **2019,** *12,* 909.

(40) Wang, X.; Zhou, W.; Li, X.; Ren, J.; Ji, G.; Du, J.; Tian, W.; Liu, Q.; Hao, A., Graphene Oxide Suppresses the Growth and Malignancy of Glioblastoma Stem Cell-like Spheroids via Epigenetic Mechanisms. *J. Transl. Med.* **2020,** *18,* 1−14.

(41) Gurunathan, S.; Han, J. W.; Eppakayala, V.; Kim, J.-H. Green Synthesis of Graphene and its Cytotoxic Effects in Human Breast Cancer Cells. *Int. J. Nanomed.* **2013,** *8,* 1015−1027.

(42) Aquilano, K.; Baldelli, S.; Ciriolo, M. R. Glutathione: New Roles in Redox Signaling for an Old Antioxidant. *Front. Pharmacol.* **2014,** *5,* 196.

(43) Ferguson, G. D.; Bridge, W. J. The Glutathione System and the Related Thiol Network in Caenorhabditis Elegans. *Redox Biol.* **2019,** *24,* 101171.

(44) Ma, B.; Wang, S.; Liu, F.; Zhang, S.; Duan, J.; Li, Z.; Kong, Y.; Sang, Y.; Liu, H.; Bu, W.; Li, L. Self-Assembled Copper–Amino Acid Nanoparticles for in Situ Glutathione "AND" H2O2 Sequentially Triggered Chemodynamic Therapy. *J. Am. Chem. Soc.* **2019,** *141,* 849−857.

(45) Zhu, X.; Shah, P.; Stoff, S.; Liu, H.; Li, C. A Paper Electrode Integrated Lateral Flow Immunosensor for Quantitative Analysis of Oxidative Stress Induced DNA Damage. *Analyst* **2014,** *139,* 2850−2857.

(46) Zhong, H.; Yin, H. Role of Lipid Peroxidation Derived 4-hydroxynonenal (4-HNE) in Cancer: Focusing on Mitochondria. *Redox Biol.* **2015,** *4,* 193−199.

(47) Valko, M.; Izakovic, M.; Mazur, M.; Rhodes, C. J.; Telser, J. Role of Oxygen Radicals in DNA Damage and Cancer Incidence. *Mol. Cell. Biochem.* **2004,** *266,* 37−56.

(48) Yin, X.; Feng, S.; Chi, Y.; Liu, J.; Sun, K.; Guo, C.; Wu, Z. Estrogen-functionalized Liposomes Grafted with Glutathione-responsive Sheddable Chotooligosaccharides for the Therapy of Osteosarcoma. *Drug Deliv.* **2018,** *25,* 900−908.

(49) Yin, D.; Li, Y.; Lin, H.; Guo, B.; Du, Y.; Li, X.; Jia, H.; Zhao, X.; Tang, J.; Zhang, L. Functional Graphene Oxide as a Plasmid-based Stat3 siRNA Carrier Inhibits Mouse Malignant Melanoma Growth in vivo. *Nanotechnology* **2013,** *24,* 105102.

(50) Chen, G. Y.; Chen, C. L.; Tuan, H. Y.; Yuan, P. X.; Li, K. C.; Yang, H. J.; Hu, Y. C. Graphene Oxide Triggers Toll-like Receptors/autophagy Responses in vitro and Inhibits Tumor Growth in vivo. *Adv. Healthc. Mater.* **2014,** *3,* 1486−1495.

TOC